Global and Stochastic Analysis
Vol. 12 No. 1 (January, 2025)

Received: 26th July 2024 **Revised: 02nd September 2024** **Accepted: 18th September 2024**

CONVECTIVE HEAT AND MASS TRANSFER IN THREE-DIMENSIONAL MHD CASSON NANOFLUID FLOW OVER AN EXPONENTIALLY STRETCHING POROUS SHEET WITH THERMAL RADIATION AND CHEMICAL REACTION

SANJANA T D AND B LAVANYA

Abstract. This study aims to investigate 3D flow of a nanofluid created by an exponentially expanding sheet in presence of a heat source and a chemical radiation source, using principles of magnetohydrodynamics (MHD). The analysis utilizes Casson fluid model and considers the impact of a porous matrix on the behavior of Casson nanofluid. Additionally, study finds convective conditions on surface and effects of thermophoresis and Brownian motion. Nonlinear PDE governing heat, mass, and flow are transformed into interconnected nonlinear ordinary differential equations using similarity parameters. These equations are then solved using Runge-Kutta fourth-order integration scheme and the shooting method. The study also presents impact of various parameters through graphs and tables. Taking Casson fluids and Newtonian fluids allows for establishment of dual solutions. The acquired results and the outcomes from the past are compared, and the connection between the two sets of results demonstrates that there is a strong correlation between them.

1. Introduction

Convective flows involve the movement of fluids due to temperature or concentration differences, transferring heat or mass. Research has explored practical applications in industrial and natural settings, such as geothermal energy extraction, groundwater movement, oil recovery, insulation design, and pollutant dispersion. One study by Mebarek-Oudina F et al. [18] explores thermal behavior of MgO-Al_2O_3/water hybrid nanofluids within porous elliptical cavity under magnetic fields, utilizing COMSOL for analysis under the Darcy-Forchheimer-Brinkman model. It highlights the impact on heat transfer efficiency and entropy, contributing significantly to optimizing thermal systems and sustainable energy technologies. Another study by Khan SA et al. [10] explores heat transport in mixed convection Reiner-Rivlin liquid flow around stretching cylinder using the Optimal Homotopy Analysis Technique (OHAM) to observe the impact of different parameters. Ali B et al. [1] studied the mixed convective flow of hybrid nanofluid over heated disk and explored enhancement of heat transmission using

2000 *Mathematics Subject Classification.* 34B15; 76D05.

Key words and phrases. Chemical reaction; thermal radiation; Three-dimensional flow; Casson fluid; exponentially stretching sheet; Shooting technique.

mixed nanofluids in porous medium. Heat and mass transfer studies how thermal energy and mass move between different mediums due to temperature and concentration differences. It includes conduction, convection, radiation, and diffusion processes and is crucial in engineering and scientific applications. Li S et al. [13, 15] researched hybrid nanofluids' heat and mass transfer properties in magnetic fields. Their findings indicated that engine oil is superior for heat transfer, whereas water-based nanofluids excel in mass transfer applications. Further investigations compared heat and mass transfer profiles and rates of MgO-Al_2O_3/water nanofluids with those of hybrid and MgO-Al_2O_3/water nanofluids. Galal AM et al. [7] studied heat and mass transfer in MHD nano liquid flow, incorporating thermal radiation, chemical reactions in nanofluids, velocity profiles, and numerical results.

Nanofluid is an advanced engineered fluid formulated through the dispersion of nano-sized particles (1-100 nanometres), including metals, non-metals, and their oxides, into a conventional or base fluid. This innovative approach markedly improves the fluid's thermal conductivity and heat transfer capability. Nanofluids have many applications in industrial cooling and heating, the automotive industry, electronics, biomedical applications, and energy-related fields. Li S et al. [14] utilized self-similarity transformation to investigate heat transfer in Maxwell nanofluid flow over porous rotating disk. They studied how different factors affected the fluid's heat transfer efficiency, providing valuable insights for transportation, architectural design, oil recovery, and medical applications. Bouzennada T et al. [4] studied nanofluid heat transfer in microchannels with flexible baffles to examine the impact of baffle shape on cooling performance and heat transfer. Kodi R et al. [11] studied mixed convection flow of Maxwell nanofluid through a vertical cone and found reduced velocity with increased Maxwell and magnetic parameters.

A porous sheet is a material with tiny pores that allow fluid to pass through. In theoretical research, Darcy's law explains flow rate through porous materials, with porosity and permeability impacting flow behavior. Marnica V et al. [17] focused on second-grade non-Newtonian fluids and used the Optimal Homotopy Asymptotic Method (OHAM) to analyze heat transfer and flow phenomena involving viscoelastic parameters, thermal radiation, and convective boundary conditions. In a study by Mahesh R et al. [16], the impact of radiation on MHD couple stress hybrid nanofluid flow was explored, and analytical solutions were derived using hypergeometric functions. Vishalakshi AB et al. [22] investigated MHD Casson fluid flow with porous medium using nanofluid, and their findings concluded variations in velocity, temperature, and heat flux.

MHD deals with dynamics of electrically conducting fluids and interaction of magnetic fields with movement of such fluids, resulting in generation of currents and exertion of forces on fluid, as well as changes to magnetic field. The MHD equations combine Navier–Stokes equations of fluid dynamics and Maxwell's equations of electromagnetism. Islam MR et al. [8] studied MHD Casson fluid flow with Brownian and thermophoresis effects, analyzing the impact of the thermal convective parameter on skin friction and the Casson term, as well as chemical processes and applications in various fields. Khan KA et al. [9] examined the behavior of a time-varying MHD Williamson nanofluid flowing over a stretched

plate, explicitly focusing on heat and mass transport properties and the influence of external factors on heat and mass transfer characteristics. Sadighi S et al. [20] conducted a study on MHD nanofluid flow, considering various influencing factors, and provided exact solutions for energy and mass transfer equations using $CoFe_2O_4/H_2O$ nanofluid, with a focus on thermal radiation and chemical reaction.

Thermal radiation, emission of electromagnetic waves from an object's surface due to its temperature, is a significant factor in heat transfer within fluid dynamics. Chemical reactions within this context involve the transformation of chemical species, influencing dynamics and properties of the system. Extensive studies have investigated consequence of thermal radiation and chemical reactions on fluid flow dynamics. Bhavya Tripathi et al. [3] found that both flow rate and flow impedance decrease as the values of the radiation parameter increase in their study of two-phase blood flow through a stenosed artery. Mansi Mishra et al. [19] predicted that the temperature profile decreases with rising radiation factor, while the induced magnetic field exhibits the opposite pattern in their investigation of MHD flow through a permeable medium. Cédric Gervais Njingang Ketchat et al. [5] analyzed the instability of MHD mixed convection flow of nanofluid in a porous channel, observing that the increase in the chemical reaction parameter decreased the values of transition Reynolds number, showing that chemical reaction sustained the instabilities. Muhammad Shoaib Anwar et al.[2] discussed the impact of generalized viscoelastic flow with thermal radiations and chemical reactions, noting that velocity, temperature, and concentration change with the variation of fractional order derivatives which was not possible with classical derivatives. Additionally, M. Vinodkumar Reddy et al. [21] studied the effects of heat source and Joule heating on convective MHD stagnation point flow of Casson nanofluid through a porous medium with chemical reaction, while Lavanya B et al. [12] explored entropy generation minimization in the Carreau nanofluid flow over a convectively heated inclined plate with quadratic thermal radiation and chemical reaction: A Stefan blowing... This paper investigates three-dimensional steady incompressible mixed-heat-flow (MHD) of Casson nanofluid over an exponentially stretched sheet with convective boundary conditions, considering radiation and heat effects. The study considers Brownian motion and thermophoresis effects in flow region and solves nonlinear ordinary differential equations using Runge Kutta method and shooting approach. Additionally, a detailed comparison between Newtonian and non-Newtonian fluids is provided, along with information on how their behaviours can be represented through graphs.

2. Mathematical formulation

This study examines steady, incompressible, three-dimensional flow of a Casson nanofluid in a porous medium over an exponentially stretched surface. The flow is affected by convective boundary conditions, radiation, chemical reactions, and heat sources. The fluid is electrically conducting under a uniform magnetic field B_0 applied along z-direction. Due to low Reynolds number, induced magnetic field is disregarded. Furthermore, study considers effects of thermophoresis and Brownian motion.Physical depiction of the flow problem is illustrated in Figure 1.

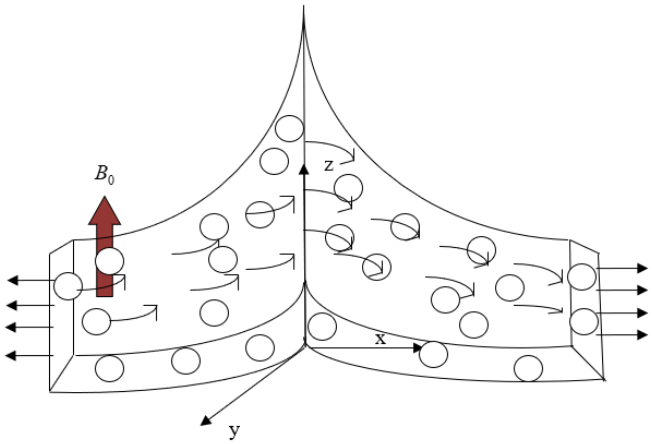

FIGURE 1. Physical Models.

For an isotropic and incompressible flow, Casson fluid's behavior is described by specific rheological equation of state.

$$\tau_{ij} = \begin{bmatrix} 2\left(\mu_B + \frac{p_y}{\sqrt{2\pi}}\right) e_{ij} & \text{if } \pi > \pi_e \\ 2\left(\mu_B + \frac{p_y}{\sqrt{2\pi_e}}\right) e_{ij} & \text{if } \pi_e > \pi \end{bmatrix}$$

where μ_B is plastic dynamic viscosity of non-Newtonian fluid, p_y is yield stress of fluid, pi is product of component of deformation rate with itself, $\pi = e_{ij}e_{ij}$, e_{ij} is $(i,j)^{th}$ component of deformation rate and π_c is critical value of this product, based on non-Newtonian model. Under these assumptions, equations governing flow can be written as

The dynamic viscosity of non-Newtonian fluid is denoted by μ_B, yield stress of fluid is denoted by p_y, product of component of deformation rate with itself is represented by $\pi = e_{ij}e_{ij}$, the i-th component of the deformation rate, π_c is component of deformation rate and is a critical value of this product, based on non-Newtonian model. Based on these assumptions, we can express equations that govern the flow as follows:

$$\frac{\partial u}{\partial x} + \frac{\partial v}{\partial y} + \frac{\partial w}{\partial z} = 0 \tag{1}$$

$$u\frac{\partial u}{\partial x} + v\frac{\partial u}{\partial y} + w\frac{\partial u}{\partial z} = v_f\left(1 + \frac{1}{\beta}\right)\frac{\partial^2 u}{\partial z^2} - \frac{\sigma B_0^2 u}{\sigma_f} - \frac{v_f u}{K^*} \tag{2}$$

$$u\frac{\partial u}{\partial x} + v\frac{\partial u}{\partial y} + w\frac{\partial u}{\partial z} = v_f\left(1 + \frac{1}{\beta}\right)\frac{\partial^2 v}{\partial z^2} - \frac{\sigma B_0^2 v}{\sigma_f} - \frac{v_f v}{K^*} \tag{3}$$

$$u\frac{\partial T}{\partial x}+v\frac{\partial T}{\partial y}+w\frac{\partial T}{\partial z}=\alpha_f\frac{\partial^2 T}{\partial z^2}+\tau\left[D_B\frac{\partial C}{\partial z}\frac{\partial T}{\partial z}+\frac{D_T}{T_\infty}\left(\frac{\partial T}{\partial z}\right)^2\right]-\frac{1}{(\rho C)_f}\left(\frac{\partial q_r}{\partial z}\right)+\frac{Q_0}{(\rho C)_f}(T-T_\infty) \tag{4}$$

$$u\frac{\partial C}{\partial x}+v\frac{\partial C}{\partial y}+w\frac{\partial C}{\partial z}=D_B\frac{\partial^2 C}{\partial z^2}+\frac{D_T}{T_\infty}\frac{\partial^2 T}{\partial z^2}-Kr(C_w-C_\infty) \tag{5}$$

The boundary conditions are as follows:

$$\begin{aligned} &u=U_w=U_0e^{\left(\frac{x+y}{L}\right)}, \quad v=v_w=v_0e^{\left(\frac{x+y}{L}\right)}, \quad w=-k_f\left(\frac{\partial T}{\partial z}\right)=h_f(T_f-T), \quad C=C_w \quad \text{at } z=0,\\ &u\to 0, \qquad\qquad v\to 0, \qquad\qquad T\to T_\infty, \qquad\qquad C\to C_\infty \quad \text{as} \quad z\to\infty \end{aligned} \tag{6}$$

where, $\alpha_f=\frac{k_f}{(\rho c)_f}, \tau=\frac{(\rho C)_\rho}{(\rho C)_f}$ utilizing Rosseland Approximation,

$$q_r=-\frac{4\sigma^*}{3k^*}\frac{\partial T^4}{\partial y}=\frac{16}{3}\frac{\sigma * T_\infty^3}{(\rho C)_f k^*}\frac{\partial^2 T}{\partial z^2}$$

On inducing similarity transformations

$$\left.\begin{aligned} &u=U_0e^{\frac{x+y}{L}}f'(\xi), v=U_0e^{\frac{x+y}{L}}g'(\xi), w=-\sqrt{\tfrac{v_fU_0}{2L}}e^{\frac{x+y}{2L}}\left[f(\xi)+\xi f'(\xi)+g(\xi)+\xi g'(\xi)\right]\\ &\xi=z\sqrt{\tfrac{U_0}{2V_fL}}e^{\frac{x+y}{L}}, \theta(\xi)=\tfrac{T-T_\infty}{T_w-T_\infty}, \phi(\xi)=\tfrac{C-c_\infty}{C_w-C_\infty} \end{aligned}\right\} \tag{7}$$

Here, continuity equation is satisfied by u, v and w. Equations (2) to (6) become

$$\left(1+\frac{1}{\beta}\right)f''+(f+g)f''-2(f'+g')f'-(M+K)f'=0 \tag{8}$$

$$\left(1+\frac{1}{\beta}\right)g''+(f+g)g''-2(f'+g')g'-(M+K)g'=0 \tag{9}$$

$$\left(1+\frac{4R}{3}\right)\theta''+Pr\left[(f+g)\theta'+Nb\theta'\phi'+Nt\theta'^2+Q\theta\right]=0 \tag{10}$$

$$\phi''+Sc(f+g)\phi'+\frac{Nt}{Nb}\theta'-Sc\gamma\phi=0 \tag{11}$$

The following are respective boundary conditions

$$\begin{aligned} &f(0)=0, \quad g(0)=0, \quad f'(0)=1, \quad g'(0)=\delta,\\ &\theta'(0)=-Bi(1-\theta(0)), \quad \phi(0)=1,\\ &f'(\infty)\to 0, \quad g'(\infty)\to 0, \quad \theta(\infty)\to 0, \quad \phi(\infty)\to 0 \end{aligned} \tag{12}$$

where, $M=\frac{2\sigma B_0^2L}{\rho_fU_w}$, $K=\frac{2v_fL}{U_wk^*}$, $\delta=\frac{V_0}{U_0}$, $R=\frac{4\sigma^*T_\infty^3}{k^*k}$, $Pr=\frac{v_f}{\alpha_f}$, $Nb=\frac{\tau D_B(C_w-C_\infty}{v_f}$,
$Nt=\frac{\tau D_B(T_f-T_\infty)}{T_\infty v_f}$, $Q=\frac{2Q_0L}{U_w(\rho C)_f}$, $Bi=\frac{h_f}{k_f}\sqrt{\frac{2U_fL}{U_w}}$, $Sc=\frac{v_f}{D_B}$, $\gamma=\frac{k_r}{v_0}$
C_{fx} and C_{fy} are dimensionless skin-friction coefficients in the directions of x and y, respectively. Sh_x denotes the local Sherwood Number, and Nu_x represents the local Nusselt Number.
$C_{fx}=\frac{2\tau_{wx}}{\rho_fU_w}$, $C_{fy}=\frac{2\tau_{wy}}{\rho_fU_w^2}$ where, $\tau_{wy}=\mu_f\left(1+\frac{1}{\beta}\right)\left(\frac{\partial u}{\partial z}+\frac{\partial w}{\partial x}\right)_{z=0}$,
$\tau_{wy}=\mu_f\left(1+\frac{1}{\beta}\right)\left(\frac{\partial v}{\partial z}+\frac{\partial w}{\partial y}\right)_{z=0}$, $Nu_x=\frac{xq_w}{k_f(T_f-T_\infty)}$,

$q_w = -\left(k_f + \left(\frac{16\sigma^* T_\infty^3}{3k^*}\right)\left(\frac{\partial T}{\partial z}\right)_{z=0}\right)$ and $Sh_x = \frac{xq_m}{D_B(C_w - C_\infty)}$, $q_m = -D_B\left(\frac{\partial C}{\partial z}\right)_{z=0}$
substituting q_w and q_m in prior equations, we get
$\left(\frac{Re}{2}\right)^{\frac{1}{2}} C_{fx} = \left(1 + \frac{1}{\beta}\right) f''(0)$, $\left(\frac{Re}{2}\right)^{\frac{1}{2}} C_{fy} = \left(1 + \frac{1}{\beta}\right) g''(0)$, $\left(\frac{Re}{2}\right)^{-\frac{1}{2}} \frac{L}{x} Nu_x = -\left(1 + \frac{4}{3}R\right)\theta'(0)$
and $\left(\frac{Re}{2}\right)^{-\frac{1}{2}} \frac{L}{x} Sh_x = -\phi'(0)$
where, $Re = \frac{U_w L}{v_f}$ is local Reynold's number.

3. Numerical process

To solve transformed Equations (8)– (11) with boundary conditions (12) as IVP:

i. Initial guess values of $f''(0)$, $g'(0), \theta'(0)$ and $\phi'(0)$ are selected.
ii. Next step is to apply Runge-Kutta-Fehlberg method to obtain required solution.
iii. $f'(\eta), g(\eta), \theta(\eta)$ and $\phi(\eta)$ determined values at $\eta = \eta_\infty (\eta_\infty$ refers sufficient large value of $\eta)$, compared with boundary conditions.
$f'(\infty) \to 0, \quad g'(\infty) \to 0, \quad \theta(\infty) \to 0, \quad \phi(\infty) \to 0.$
iv. for $f''(0), g'(0), \theta'(0)$ and $\phi'(0)$ missing values, shooting method is utilized.
v. We have fixed $K, M, \delta, R, Pr, Bi_1, Sc$, and γ.
vi. With help of MATHEMATICA 11.0 software for various $\Delta\eta$ size values, velocity, temperature, skin friction coefficient, and local Nusselt number changed negligibly for value of $\Delta\eta > 0.01$. Consequently, step-size $\Delta\eta = 0.001$ has been determined by the authors

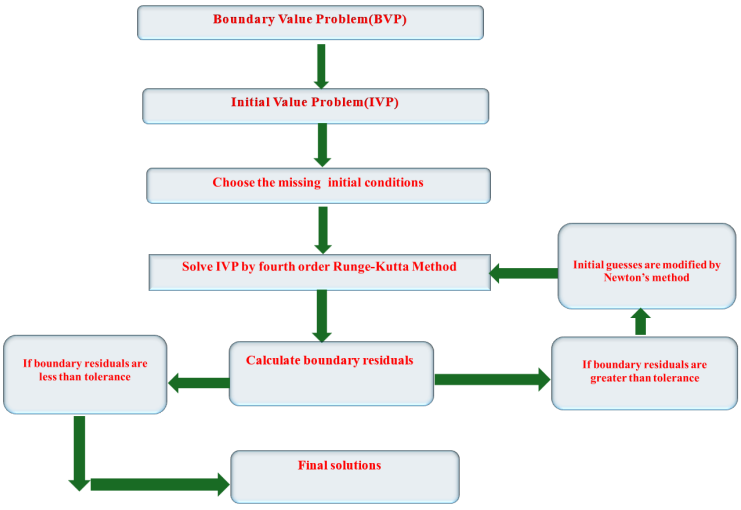

FIGURE 2. Flow chart representation of numerical method

4. Results and Discussion

Here we present few findings that shed light on the issue. Here are some findings that provide insight into the issue. All values, except for the updated numbers presented in tables and graphs, are considered for these calculations throughout the investigation. The outcomes are derived for Casson and Newtonian fluids.

Due to fact that Lorentz force exerts its resistance on motion of fluid, axial and transverse velocities of fluid are slowed down with utilisation of Hartmann parameter M. The figures 3 and 4 illustrate this point. The velocities in both directions are shown to decrease when porosity parameter K increases, as seen in Figures 5 and 6. It is because of the Darcy resistance that porous medium offers that this is case. A visual representation of effect that ratio parameter has on both velocities can be found in Figures 7 and 8. The amplification in indicates a significant stretching rate in x-direction, and as a result, velocity in y-direction increases, while velocity in x-direction decreases in proportional manner. Rise in Prandtl number Pr is equivalent to decrease in temperature field value. As a result of fact that a Prandtl number that is physically bigger has a weaker thermal diffusivity, temperature that is seen in Figure 9 is lower. Observations indicate that an increase in radiation parameter R can strengthen thermal boundary layer, leading to gradual rise in fluid temperature, as shown in figure 10. In Figure 11, it is shown that increasing Biot number, Bi, causes temperature rise. When Biot number increases, it leads to higher heat transfer coefficient, transferring more thermal energy to fluid, thus increasing temperature. A heat source parameter, Q in fluid releases thermal energy, raising temperature accordingly. Figure 12 depicts this effect. The impact of Brownian motion, Nb, and thermophoresis parameters, Nt, on temperature field, is demonstrated in Figures 13 and 14, respectively. These characteristics result from the presence of nanoparticles, which enhance thermal conductivity of the fluid, leading to a temperature increase with increasing values of parameters Nb and Nt. A comparison with the Casson fluid shows that influence of these parameters is significantly more significant in Newtonian fluid.

The effects of Brownian motion and thermophoresis parameters on concentration field can be observed in Figures 15 and 16, respectively. An increase in values of parameters demonstrates higher thermophoretic force, causing nanoparticles to move from hot sheet into quiescent fluid, resulting in an increase in nanoparticle volume fraction boundary layer, thus improving focus. However, an increase in Brownian motion parameter has shown opposite phenomenon in concentration profiles.

The impact of Schmidt number (Sc) and chemical reaction parameter γ on concentration patterns is illustrated in Figures 17 and 18, showing that concentration decreases as values of Sc increases, due to weakening of the Brownian coefficient. In Figures 19 and 20, it is evident that skin friction coefficients decrease as magnetic parameter (M) and porous parameter (K) increase. This trend is quite noticeable. Furthermore, it is noticed from Fig. 21 that both Biot number and radiation parameter (R) contribute to increase in local Nusselt number. Additionally, increase in Schmidt number leads to rise in Sherwood number, whereas

increase in thermophoresis parameter results in decrease in Sh_x, as illustrated in Fig.22.

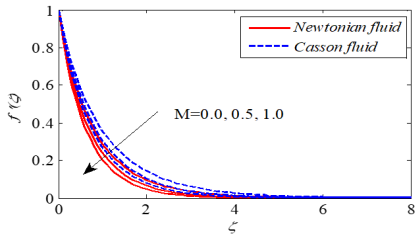

FIGURE 3. Effect of M on $f'(\xi)$

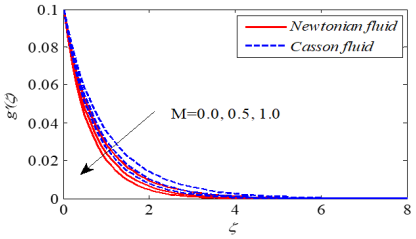

FIGURE 4. Effect of M on $g'(\xi)$

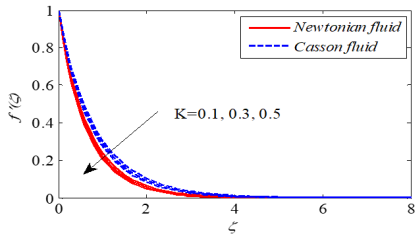

FIGURE 5. Influence of K on $f'(\xi)$

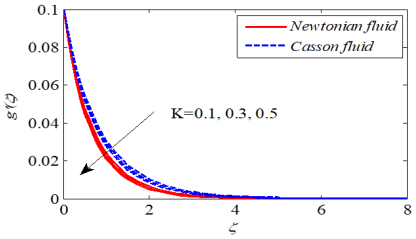

FIGURE 6. Influence of K on $g'(\xi)$

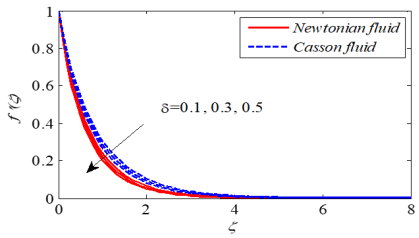

FIGURE 7. Influence of δ on $f'(\xi)$

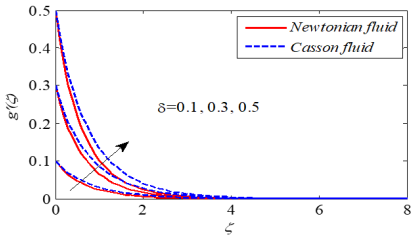

FIGURE 8. Influence of δ on $g'(\xi)$

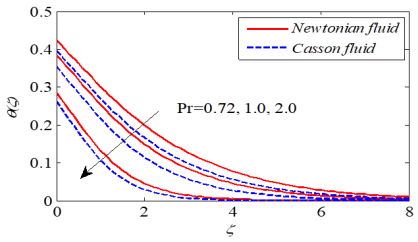

FIGURE 9. Effect of Pr on $\theta'(\xi)$

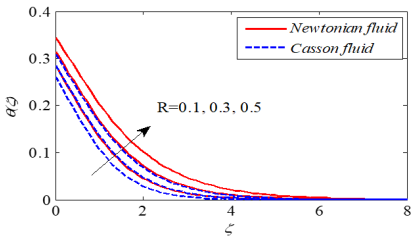

FIGURE 10. Effect of R on $\theta'(\xi)$

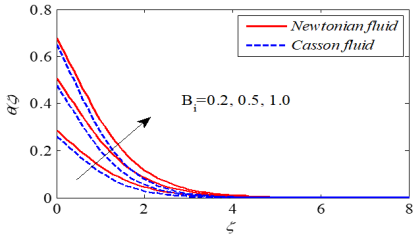

FIGURE 11. Effect of B_i on $\theta'(\xi)$

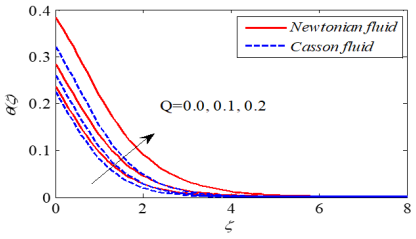

FIGURE 12. Effect of Q on $\theta'(\xi)$

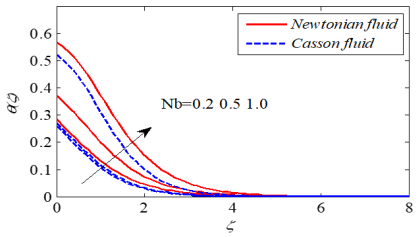

FIGURE 13. Effect of Nb on $\theta'(\xi)$

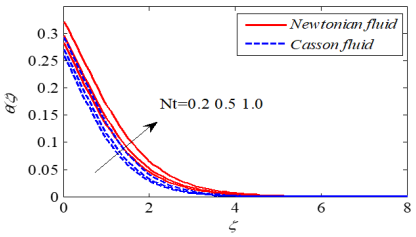

FIGURE 14. Effect of Nt on $\theta'(\xi)$

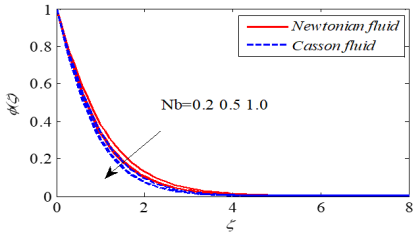

FIGURE 15. Effect of Nb on $\phi'(\xi)$

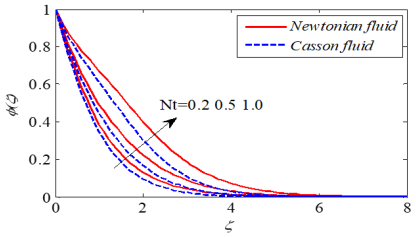

FIGURE 16. Effect of Nt on $\phi'(\xi)$

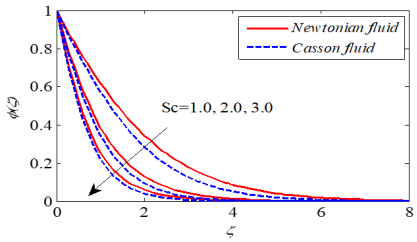

FIGURE 17. Influence of Sc on $\phi'(\xi)$

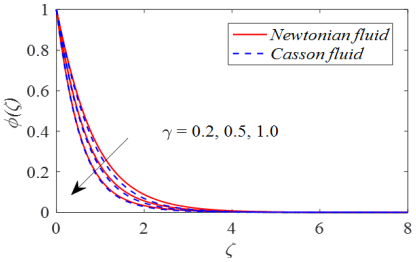

FIGURE 18. Effect of γ on $\phi'(\xi)$

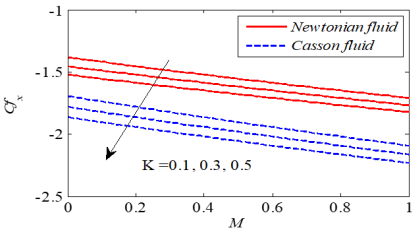

FIGURE 19. Influence of M and K on C_{fx}

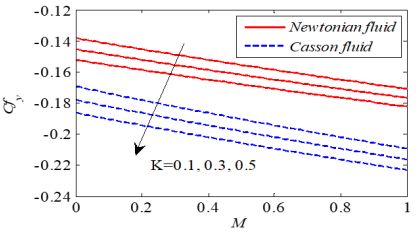

FIGURE 20. Effect of M and K on C_{fy}

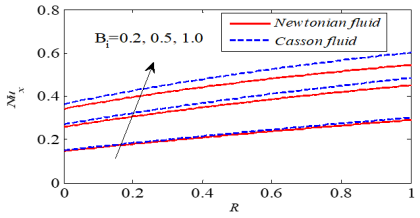

FIGURE 21. Influence of B_i and R on Nu_x

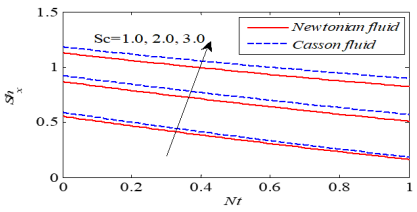

FIGURE 22. Effect of Nt and Sc on Sh_x

To validate the current analysis, we compared results of $-f''(0)$ and $-g''(0)$ with those of Chung Liu et al.[6] for limiting case $M = K = 0.0$ and $\beta \to \infty$

Δ	**Chung Liu et al.**[6]		**Present values**	
	$-f''(0)$	$-g''(0)$	$-f''(0)$	$-g''(0)$
0.0	1.28180856	0	1.2818267	0
0.5	1.56988846	0.78494423	1.569888	0.784948
1.0	1.81275105	1.81275105	1.812757	1.812759

5. Conclusions

A thorough investigation into three-dimensional steady incompressible mixed-heat-flow (MHD) of Casson nanofluid across exponentially stretched sheet with convective boundary conditions, subjected to radiation and heat, is carried out in this work. The flow region considers Brownian motion and thermophoresis effects. When solving nonlinear ODEs, RK method and firing approach are employed. Main conclusions drawn from study are as follows:

- As values of increases, there is decrease in axial velocity, whereas transverse velocity shows the opposite tendency.
- When contrasted with Casson fluid, Newtonian fluid exhibits a far higher impact of Nb and Nt.
- Concentration field is expected to be slowed down by the Schmidt number.
- The temperature field of Newtonian fluid is more affected by an increase in radiation parameter than that of Casson fluid.

Nomenclature

u, v, w	Components of velocity along x and y direction
M	Hartmann Number
v_f	Kinematic viscosity
Q_0	Heat source coefficient
B_0	Uniform magnetic field strength
δ	Ratio parameter
σ	Base fluid's electrical conductivity
Pr	Prandtl number
ρ_f	Density of fluid
Nb	Brownian motion parameter
K^*	Permeable parameter
Nt	Thermophoresis parameter
α_f	Diffusivity parameter
R	Radiation parameter
τ	Ratio between nanoparticle material's effective heat capacity and fluid's heat capacity
K	Non-dimensional porous parameter
T	Temperature
Q	Parameter of heat source
C	Nanoparticle concentration
Sc	Schmidt number
q_r	Radiative heat flux
Re	Local Reynold's number
T_f	Temperature of convective fluid below sheet
Bi	Biot number
C_w	Concentration of nanoparticle at surface of sheet
μ_f	Dynamic viscosity of fluid

T_∞	Ambient fluid's temperature
q_w	Wall heat flux
C_∞	Ambient nanoparticle concentration
q_m	Wall mass flux
β	Casson fluid particle
τ_{wx}, τ_{wy}	Shear stress along direction of x and y
D_B	Brownian diffusion coefficient
$f'(\cdot), g'(\cdot)$	Velocity profiles
U_w, V_w	Stretching velocities
ϕ	Concentration profiles
U_0, V_0	Reference velocities
C_{fx}, C_{fy}	Skin-friction coefficients along x and y directions
h_f	Convective heat transfer coefficients of fluid
Nu_x	Local Nusselt number
k_f	Fluid's thermal conductivity
Sh_x	Sherwood number
L	Reference length
k^*	Mean absorption coefficient
σ^*	Stefan-Boltzmann constant
γ	Chemical reaction parameter

References

1. Ali B, Mishra NK, Rafique K, Jubair S, Mahmood Z, Eldin SM.: Mixed convective flow of hybrid nanofluid over a heated stretching disk with zero-mass flux using the modified Buongiorno model. *Alexandria Engineering Journal.,* **72** (2023), 83-96.
2. Anwar MS, Alam MM, Khan MA, Abouzied AS, Hussain Z, Puneeth V. Generalized viscoelastic flow with thermal radiations and chemical reactions. *Geoenergy Science and Engineering.* **232** (2024).
3. Bhavya Tripathi and Bhupendra Kumar Sharma.: Two-phase analysis of blood flow through a stenosed artery with the effects of chemical reaction and radiation. *Ricerche di Matematica.,* **73** (2024),151–177.
4. Bouzennada T, Fteiti M, Alshammari BM, Hadrich B, Kriaa K, Maatki C, Kolsi L. :Numerical study on nanofluid heat transfer and fluid flow within a micro-channel equipped with an elastic baffle.*Case Studies in Thermal Engineering.,* **1**(56), (2024)
5. Cédric Gervais Njingang Ketchate , Pascalin Tiam Kapen , Didier Fokwa and Ghislain Tchuen.: Instability of MHD mixed convection flow of nanofluid in porous channel with thermal radiation, chemical reaction, Dufour and Soret effects. *Chinese Journal of Physics.,* **87** (2024),728-750
6. Chung Liu I, Hung-Hsun Wang and Yih-Ferng Peng:, Flow and heat transfer for three dimensional flow over an exponentially stretching surface., *Chemical Engineering Communications.,***200**, (2014),253-268.
7. Galal AM, Alharbi FM, Arshad M, Alam MM, Abdeljawad T, Al-Mdallal QM.: Numerical investigation of heat and mass transfer in three-dimensional MHD nanoliquid flow with inclined magnetization., *Scientific reports.* **14**(1207), (2024).
8. Islam MR, Biswas R, Hasan M, Afikuzzaman M, Ahmmed SF. : Modeling of MHD casson fluid flow across an infinite vertical plate with effects of brownian, thermophoresis, and chemical reactivity., *Arabian Journal for Science and Engineering.,* **49** (2024), 11139–11156.
9. Khan KA, Javed MF, Ullah MA, Riaz MB.: Heat and Mass transport analysis for Williamson MHD nanofluid flow over a stretched sheet.*Results in Physics.* **53**, (2023).

10. Khan SA, Razaq A, Alsaedi A, Hayat T. Modified thermal and solutal fluxes through convective flow of Reiner-Rivlin material. *Energy.,* **283**, (2023).
11. Kodi R, Ganteda C, Dasore A, Kumar ML, Laxmaiah G, Hasan MA, Islam S, Razak A.: Influence of MHD mixed convection flow for maxwell nanofluid through a vertical cone with porous material in the existence of variable heat conductivity and diffusion. *Case Studies in Thermal Engineering.*, **44**,(2023).
12. Lavanya B, Kumar JG, Babu MJ, Raju CS, Almutairi B, Shah NA. Entropy generation minimization in the Carreau nanofluid flow over a convectively heated inclined plate with quadratic thermal radiation and chemical reaction: A Stefan blowing application. *Propulsion and Power Research.,* **13**(2) (2024),233-44.
13. Li S, Abbasi A, Farooq W, Gul M, Khan MI,Nafasova G, Hejazi HA. Heat and mass transfer characteristics of Al2O3/H2O and (Al2O3+ Ag)/H2O nanofluids adjacent to a solid sphere: A theoretical study.: *Numerical Heat Transfer, Part A: Applications.,* (2024), 1-9.
14. Li S, Faizan M, Ali F, Ramasekhar G, Muhammad T, Khalifa HA, Ahmad Z. Modelling and analysis of heat transfer in MHD stagnation point flow of Maxwell nanofluid over a porous rotating disk.: *Alexandria Engineering Journal.* **91** (2024),237-48
15. Li S, Saadeh R, Madhukesh JK, Khan U, Ramesh GK, Zaib A, Prasannakumara BC, Kumar R, Ishak A, Sherif ES. : Aspects of an induced magnetic field utilization for heat and mass transfer ferromagnetic hybrid nanofluid flow driven by pollutant concentration. *Case Studies in Thermal Engineering.,* **53** (2023).
16. Mahesh R, Mahabaleshwar US, Kumar PV, Öztop HF, Abu-Hamdeh N.: Impact of radiation on the MHD couple stress hybrid nanofluid flow over a porous sheet with viscous dissipation. *Results in Engineering.***17**, (2023)
17. Marinca V, Marinca B, Herisanu N.:Study of heat transfer in MHD viscoelastic fluid of second grade over a stretching porous sheet with electromagnetic effects and nonuniform source/sink. *Journal of Computational and Applied Mathematics.,* **439** (2024)
18. Mebarek-Oudina F, Chabani I, Vaidya H, Ismail AA.: Hybrid-nanofluid magneto-convective flow and porous media contribution to entropy generation. *International Journal of Numerical Methods for Heat & Fluid Flow.,* **34**(2) (2024),809-36.
19. Mishra M, Panda JP, Sahoo SS. :Investigations concerning the effects of thermal radiation, induced magnetic field, and chemical reaction on MHD flow through a permeable medium. *International Journal of Modern Physics.,* **38**(02),(2024).
20. Sadighi S, Afshar H, Jabbari M, Ashtiani HA.: Heat and mass transfer for MHD nanofluid flow on a porous stretching sheet with prescribed boundary conditions. *Case Studies in Thermal Engineering.* **49**, (2023).
21. Vinodkumar Reddy M, Vajravelu K, Lakshminarayana P, Sucharitha G.: Heat source and Joule heating effects on convective MHD stagnation point flow of Casson nanofluid through a porous medium with chemical reaction. *Numerical Heat Transfer, Part B: Fundamentals.,* **85**(3), (2023), 286-304.
22. Vishalakshi AB, Mahabaleshwar US, Ahmadi MH, Sharifpur M. : An MHD Casson fluid flow past a porous stretching sheet with threshold Non-Fourier heat flux model. *Alexandria Engineering Journal.* **69** (2023),727 -37.

Sanjana T D:Department of Mathematics, Manipal Institute of Technology, Manipal Academy of Higher Education, Manipal-576104, Karnataka, India.
Email address: sanjanadevis128@gmail.com

B Lavanya:Department of Mathematics, Manipal Institute of Technology, Manipal Academy of Higher Education, Manipal-576104, Karnataka, India.
Email address: lavanyab2015@gmail.com